Korean J. Chem. Eng., 39(3), 775-784 (2022)
DOI: 10.1007/s11814-021-0953-7

pISSN: 0256-1115
eISSN: 1975-7220

Highly durable spray-coated superhydrophobic surface: Pre-anodizing and fatty acid chain length effect

Omur Aras, Enver Baydir†, and Bugra Akman

Bursa Technical University, Faculty of Engineering and Natural Sciences, Department of Chemical Engineering, Turkey
(*Received 4 July 2021 • Revised 19 August 2021 • Accepted 5 September 2021*)

Abstract−In the study, aluminum plates were first anodized and then coated with ZnO by spray-pyrolysis method. By modification with long chain fatty acid, these surfaces demonstrate superior hydrophobicity and durability. After optimizing the anodizing time for each fatty acid, several runs were conducted by varying concentration and spray solution quantity. Comparison was made by optimizing the process parameters in which each acid showed maximum hydrophobicity. Anodized, spray coated and modified surfaces were characterized by FT-IR, XRD, SEM and topography analysis. The chemical and mechanical strength of the surfaces were explored under various extreme conditions. The highest contact angle of 164° was obtained by coating 10 minutes anodized surface with 0.4 M and 15 ml $ZnNO_3$ solution and modifying it with stearic acid. In the performed tests, it has been observed that this surface is much more durable than surfaces modified with other fatty acids.

Keywords: Superhydrophobic, Spray Pyrolysis, Durability, Long Chain Fatty Acids, Anodizing Effect

INTRODUCTION

Some natural surfaces, such as the lotus leaf and butterfly wing, have naturally superhydrophobic properties. Such surfaces have the unusual wetting property of superhydrophobicity with a contact angle greater than 150° [1]. From this point of view, surfaces with a contact angle greater than 150° and a sliding angle less than 10° are defined as superhydrophobic surfaces [2]. The superhydrophobic behavior of any surface cannot be produced by surface chemistry alone. Two different views have been proposed to explain this effect. The first is the Wenzel model. According to this model, the roughness of the surface increases the surface area of the solid, which geometrically increases the hydrophobicity. Another model is the Cassie model. In this model, air can become trapped under the water drop. This leads to superhydrophobic behavior because the droplet has a partial floating approach [3]. Superhydrophobic coatings have attracted the attention of many researchers because of their use in many fields, including anti-fog coating, anti-freezing surfaces, oil and water separation, antibacterial surfaces and medical applications [4-8]. The wettability of a solid surface is a function of two main factors: surface roughness and surface energy. The hydrophobicity of a surface is indicative of the water contact angle on the surface. In hydrophobic structures, there are air pockets between the water droplet and the microstructures on the surface. Air pockets prevent the water droplet from contacting the bottom and minimize the contact area between the droplet and the surface. This results in high contact angle and low adhesion [9]. The initial properties of the surface are also important when preparing a superhydrophobic surface. The roughness of the starting surface causes an increase in the contact angle, as it allows air pockets on the surface. Therefore, the wettability of a material is closely related to its surface hierarchy [10]. In addition, the chemical composition plays a decisive role in determining surface wettability and adhesion [11]. After the surfaces are modified with a low surface energy material, they exhibit superhydrophobic properties. This occurs at the contact angle where the thermodynamic energy is minimal. The contact angle is the result of the interaction between the tensions of the liquid-gas interface, liquid-solid interface, solid-gas interface and can be calculated by considering the force balance in the three-phase contact line [12,13].

Many methods are used for superhydrophobic surface formations, such as dip coating, electrospinning, sol-gel, chemical vapor deposition, chemical and physical etching, spray coating, and electrochemical deposition methods [14-21]. The poor mechanical strength of the superhydrophobic coating is a result of the low adhesion between the coating and the substrate. Researchers are putting great effort into the synthesis of super hydrophobic surfaces with high mechanical stability. In addition, expensive toxic reagents are generally preferred due to their low surface energies. However, some problems, such as high cost, complex preparation steps, toxicity, and narrow applicability, are obstacles to the advancement of superhydrophobic coating technology in real-life applications [22]. There are many material options for fabrication of superhydrophobic surfaces such as metallic oxides (TiO_2, ZnO, Al_2O_3, Fe_3O_4, $CoFe_2O_4$), nano coatings such as inorganic silica-based materials (SiO_2 nanoparticles, TEOS, OTES), carbon-based materials (carbon nanotubes, carbon nanotube, graphene and fullerene), metallic materials (AgCl, $AuCl_3$ etc.), nano-functional silver and gold on copper

Electronic supplementary material The online version of this article (https://doi.org/10.1007/s11814-021-0953-7) contains supplementary material, which is available to authorized users.

†To whom correspondence should be addressed.
E-mail: enver.baydir@btu.edu.tr
Copyright by The Korean Institute of Chemical Engineers.

surfaces and sulfides. Among these, ZnO is generally preferred in the first step of the superhydrophobic coating application due to its advantages such as accessibility, low cost and easy applicability. ZnO coated surface is modified with organic compounds to provide low surface energy to obtain superhydrophobic surface [13]. In the literature, palmitic, lauric and stearic acid are the most preferred fatty acids for surface modification [23-28].

Fan et al. coated zirconium palmitate on carbon fiber surface with electrochemical technique in one step. The maximum contact angle they found was 157° [29]. Zhu and Hu roughened the aluminum surface using self-made disc cutters and then modified it by stearic acid [30]. Lomga et al. first subjected the aluminum surface to chemical etching in NaOH solution, then modified with lauric acid; the highest contact angle value that they obtained was 170° [31]. Considering chemical and mechanical durability, the super hydrophobic surface obtained with spray coating has attracted the attention of researchers in recent studies. Celik et al. produced high mechanical durable superhydrophobic surfaces by the coating of nanoparticles functionalized with alkyl silane, that can withstand 45 minutes of water-jet effect [32]. In a biopolymer-based superhydrophobic surface study, Wang et al. sprayed organosoluble chitosan staroyl ester on silicon wafer and obtained chemically and mechanically resistant surfaces [33]. Golovin et al., considering that even the most durable superhydrophobic surfaces can be damaged, produced self-renewable surfaces with spray coating [34]. Similar to these studies, there are many studies aiming to preserve surface durability and super hydrophobic property for a long duration [35-42].

Different micro/nano hierarchical roughness methods, such as electrochemical etching, lithography, use of inductively coupled plasma (ICP) and hot embossing, are available in the literature [43-47]. In this study, in order to achieve roughness, which is one of the main factors of super hydrophobicity, the surface was anodized before ZnO spray coating. The effect of anodizing time on superhydrophobic property and durability was investigated in detail. The anodized plates were first spray coated with zinc nitrate solution at high temperature to form ZnO on the surface, then modified with lauric, stearic and palmitic acid separately to give them superior superhydrophobic properties. All process parameters were optimized for each fatty acid. In the literature UV lamps have different wavelengths and power was used for radiation test. Again, most pH tests in the literature are based on contact angle measurements. From this point it is difficult to make a comparison. The effect of anodizing process and fatty acid chain length on the mechanical and chemical durability was also investigated. UV, temperature, pH and abrasion tests were applied for this aim.

EXPERIMENTAL

1. Materials

In the experiments, 1050 aluminum plates with the dimensions of 50×20×1.5 mm were used as substrate. Content of the aluminum plate: 99.03% aluminum, 0.4% iron, 0.25% silicon, 0.07% zinc, 0.05% manganese, 0.05% copper, 0.05% magnesium, 0.1% chromium. Merck provided $ZnSO_4 \cdot 7H_2O$, acetone, ethanol, and long chain fatty acids (palmitic, lauric, and stearic acid) were used for all experiments. The Rigol DP832 power supply was used for the anodizing processes.

2. Anodizing Process

The aluminum plates were cleaned with ethanol and acetone before the anodizing, and then thoroughly rinsed with distilled water. For the anodizing process, the aluminum substrate was placed in an anodizing cell containing 0.1 M $NaCl_{(aq)}$ solution. The negative pole of the direct current (DC) power supply was connected to the zinc plate, which served as the cathode. The anode in the cell was an aluminum plate connected to the positive pole of the DC power supply. The anode and cathode were placed 2.5 cm apart from each other. The temperature of the magnetic stirrer's bath was kept at about 50 °C to avoid overheating. Anodizing process was carried out at different time intervals at a constant voltage (24 V). Schematic of the anodizing process is given in Fig. 1.

3. Preparation of Zn Nano-coatings by Spray Pyrolysis

Anodized aluminum plates were re-washed before spray coating. They were immersed in 0.5 M H_2SO_4 for 1 minute at room temperature and then rinsed well with deionized water and dried with high purity nitrogen (99.999%). Then spray coating process was applied. Air from the compressor was used as the carrier gas for the spray coating. The pressure of the carrier gas was set at 3 bar and its flow rate was set to 2.5 l/min. The coating temperature was kept constant at 375 °C. Spray nozzle was set at approximately 0.3 mm. Spray coating process was conducted using 0.1, 0.25, 0.4 and

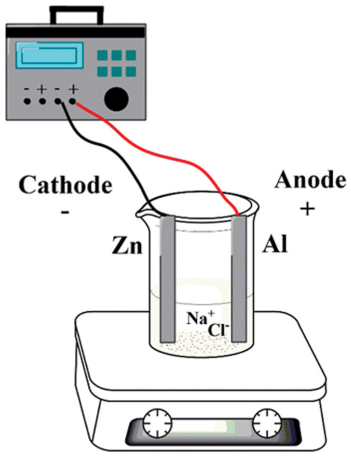


Fig. 1. Schematic demonstration of anodizing process.

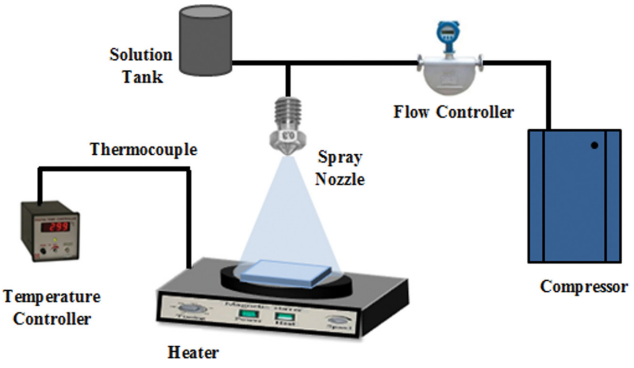


Fig. 2. Spray pyrolysis coating system.

0.6 M $ZnSO_4$ solution. Plates coated at various conditions were immersed in 0.05 M fatty acid solution and modified for 1.5 hours. Spray pyrolysis system used in the experiment is shown in Fig. 2.

4. Characterization of the Prepared Superhydrophobic Surface

Contact angles of the all samples were measured with the Attention Theta Lite brand contact angle device. Spectrum Two brand was used for FTIR analysis. Bruker AXS/Discovery D8 brand for XRD analysis, and Carl Zeiss/Gemini 300 for SEM characterization. The topography of the surface was obtained by using the Biolin Scientific/Theta Flex device.

RESULTS AND DISCUSSION

1. Anodizing Time Effect

Before exploring the anodizing time effects on superhydrophobicity, the anodizing process was not applied in any of the preliminary experiments. Each experiment was conducted three times and five measurements were taken from the different locations of the samples in all experiments. Average contact angle values were given as the result. The aluminum plate was firstly treated with SiC sandpaper up to 1,200 grit. And the washing and cleaning operation were conducted. After that 0.25 M Zinc solution was sprayed on to the substrate at various quantities of spraying solution. Contact angles values were obtained by modifying with palmitic acid as modifying agent. As shown in Table 1. the results were not satisfactory. There are no trials exhibiting super hydrophobic property.

After these experiments, the substrate was anodized before the spray pyrolysis coating to explore the anodizing effect. Different anodizing times for fixed coating concentration (0.25 M) and quantity (10 ml) were investigated as initial point. Palmitic/lauric/stearic acid were separately used to modify these surfaces.

As seen in Fig. 3, the contact angle was found to be low when the surface was anodized for 1 minute and modified with high chain fatty acid before coating. The reason for this is that the surface did not have sufficient roughness before coating. Therefore, the wettability of a material is closely related to its surface hierarchy [10].

Table 1. Contact angle values obtained by the spray pyrolysis method without anodizing step

Concentration (M)	Solution quantity (ml)	Contact angle (°)
0.25	10	148.2
0.25	15	136.9
0.25	20	138.2

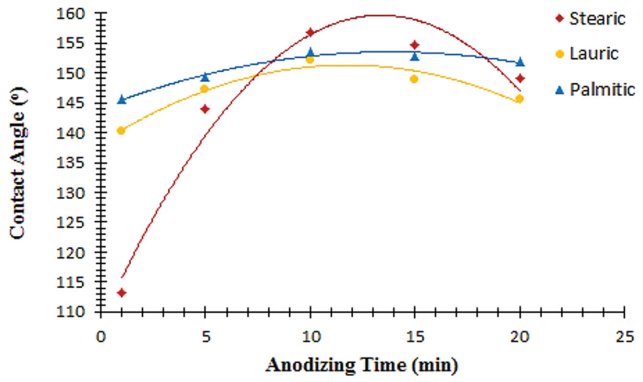


Fig. 3. Anodizing time effect on the super hydrophobicity at fixed solution concentration (0.25 M) and quantity (10 ml).

First, the 3D topography module of the contact angle measurement device was used to explore the time effect of anodizing process on the roughness. As seen from Fig. S1, the roughness of the surface increased with increasing time. A thin layer unidirectional roughness was observed on the surface after 1 and 5 minutes of the anodizing with great homogeneity. However, when the anodizing time was taken as 10 minutes, unlike the others, micro-cracks and nano-roughnesses were observed on the surface. It can be thought that this is the factor that increases the durability and higher contact angle. Because when 25 minutes anodizing time was taken, 1-dimentional roughness had changed to 2d roughness, homogeneity had increased, but the roughness level had also decreased. This caused a decrease in the contact angle compared to the 10 min anodizing time. This results in an optimal anodizing time.

The highest contact angle values were obtained for 10 minutes anodizing time. Constant 10 minutes duration was chosen as anodizing time for the next trials because all figures exhibited a concave trend, which means has an optimal value. The effects of the other parameters were investigated in the following experiments after determining 10 minutes anodizing time.

After the surface was prepared with optimum anodizing time, some operations were carried out. Surfaces with higher contact angle were obtained compared to the surfaces at other anodizing times and the non-anodized surfaces. The contact angle values of the surfaces obtained with optimum anodizing time were found to be high. Thus, it took longer time to lose its superhydrophobicity against the tests performed. Therefore, the mechanical and chemical resistance tests performed for the surface obtained at the optimum anodizing time allowed us to comment on the time-dependent durability of the surface.

2. Effect of Solution Concentration and Quantity

After anodizing process, zinc oxide spray coating process was conducted. The results obtained with different fatty acids are given in Fig. 4. The contact angle values of palmitic and stearic modified surfaces increase until the solution concentration reaches 0.4 M and then begin to decrease. This situation takes place from 0.25 M for the lauric acid modified surface.

Again, when the quantity of the solution sprayed on to the surface was increased gradually, increases in contact angles appeared in the similar trend. Additional trials were carried out at optimum concentrations for 20 ml solution. The data of these trials are given in Table 2. As can be seen, 15 ml is the optimum solution quantity. After this point, there were decreases in the contact angles. This

Table 2. Contact angle values obtained at optimal concentration and 20 ml spray solution

Fatty acid	Concentration (M)	Contact angle (°)
Stearic acid	0.4	159.7
Palmitic acid	0.4	154.7
Lauric acid	0.25	153.8

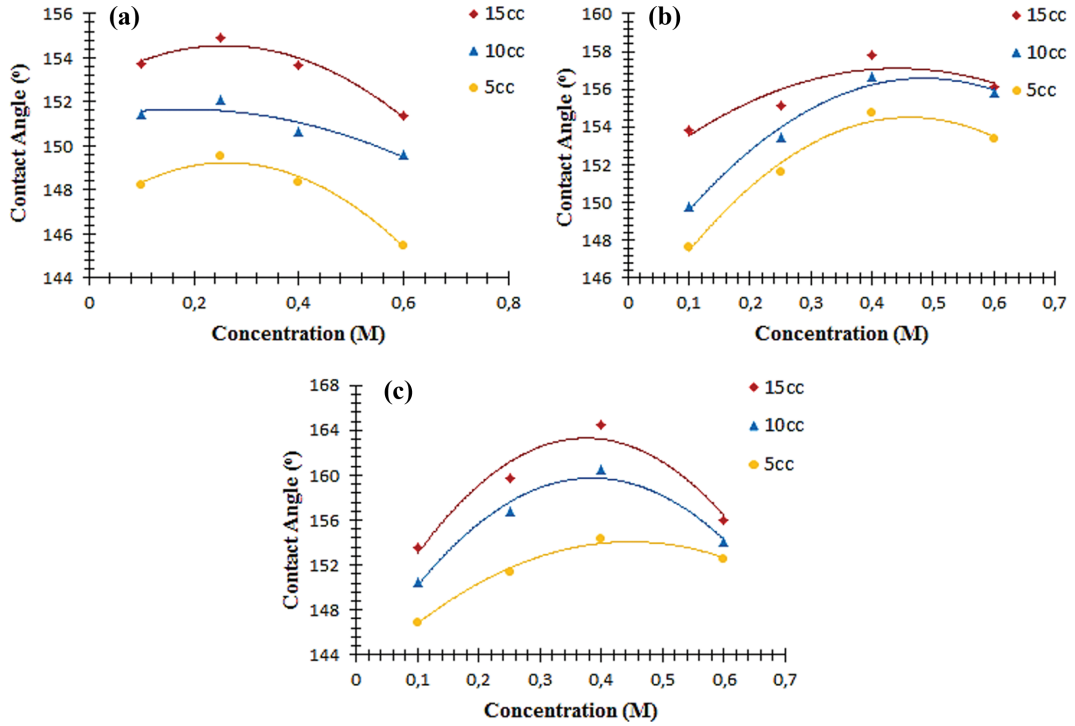


Fig. 4. Contact angles values of the (a) lauric (b) palmitic (c) stearic acid modified surfaces for different solution concentrations and quantities.

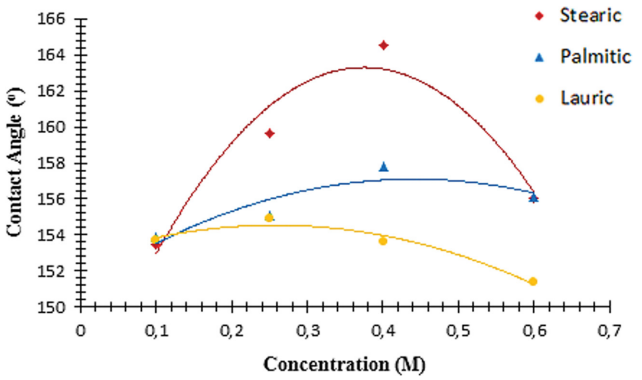


Fig. 5. Comparison curve of the different fatty acids at optimal anodizing time and solution quantity.

reduction was 3.1° for the palmitic acid, 4.5° for the stearic acid, 1.1° for the lauric acid modified surfaces. This situation is clearly seen especially from Fig. 4(b) and (c) that the peaks of the curves are getting closer each other.

The comparison curves are given in Fig. 5. As can be seen, each fatty acid exhibits its own characteristics. When 0.4 molar and 15 ml solution is sprayed on to the surface and then modified with stearic acid, 164° contact angle is obtained. This value is 158° for palmitic acid and 154° for lauric acid modified surface.

Table 3 lists the contact angle and sliding values for the best results, while the supplementary section contains their images and movies.

Now, at a fixed amount of solution, the change of concentration will affect the size and number of nanoparticles on the surface. Low concentration will form sparse and smaller nanostructures on the surface. For low nanoparticle concentrations on the surface, the contact angle results in low values. This indicates that water penetrates between the microstructures and causes the Wenzel regime to become wet. At high concentrations, the amount of substance and particle size on the surface will increase, agglomeration will begin, and therefore micro/nano roughness will disappear. Regardless of the acid chain length, the hydrophobicity will then be reduced. The interaction of the contact angle with the concentration can be explained in this way. The contact angle also depends on the chain length of the modified fatty acid [48].

The nanoparticle concentration exhibits the optimum concentration (0.25/0.4 M depends on chain length) by modification of the surface with long chain fatty acids. To show this situation, 0.1 M

Table 3. Effect of solution concentration and fatty acids on contact and sliding angle

Modifier	0.25 M-15 ml (LA)	0.4 M-15 ml (SA)	0.4 M-15 ml (PA)
Contact angle (°)	154°±0.2	164°±0.2	158°±0.2
Sliding angle (°)	~3	~0-1	~2

LA: Lauric Acid, **SA:** Stearic Acid, **PA:** Palmitic Acid

and 0.6 M spray coatings were done with 10 cc solution in 10 minutes anodizing time, then these surfaces modified with each fatty acid and analyses were carried out. SEM images of lauric, palmitic and stearic modified surfaces are given in Fig. S2(a), (b), (c), (0.1 M), respectively, and Fig. S2(d), (e), (f) (0.6 M).

At low concentrations (0.1 M), nano-roughness is noticeable. Very small differences emerged according to acid chain length. When the concentration was taken as 0.6 M, it is seen that there are sparse and few micro nanostructures on the surfaces where macro structures increase and agglomerations begin. Therefore, higher superhydrophobic contact angles are achieved at optimal solution concentrations depending on chain length. In this case, the droplet cannot or partially penetrates through the microstructures. This results in Cassie-Baxter wetting and low adhesion. The higher contact angles seen at optimal particle concentrations are likely the result of optimal nano/micro roughness on the surface. It also leads to partial wetting of the nanostructure rather than complete wetting [9,49].

Fig. S3 in the appendices shows the hydrophobicity of stearic acid modified surfaces. In addition, Fig. S4 and video A1 shows the sliding angle images of the sample modified with stearic acid. Also, Fig. S5-S7 presents the best contact angle images modified with lauric, palmitic and stearic acid, respectively.

3. Characterization

The 3D topography module of the contact angle measuring device was used to identify the surface roughness after anodizing process during the experimental studies; it was observed that all fatty acids gave optimum results in 10 minutes anodizing time. Therefore, the 2- and 3-D topography of the surface, which was anodized for 10 minutes, was examined. As shown in the Fig. 6, an anodizing time of 10 minutes caused a patterned structure in the surface. Patterned hill and valley are seen in region by region. While the micro roughness is seen on top of the surfaces (1-10 μm), the depths of the valley areas are around 30 μm. It can be

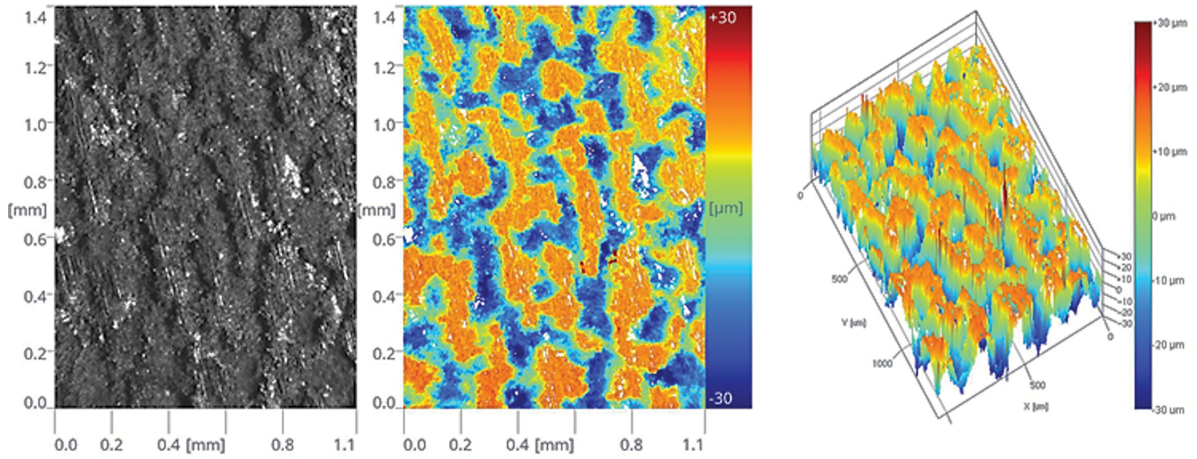


Fig. 6. Surface topography of the samples after 10 minutes anodizing process.

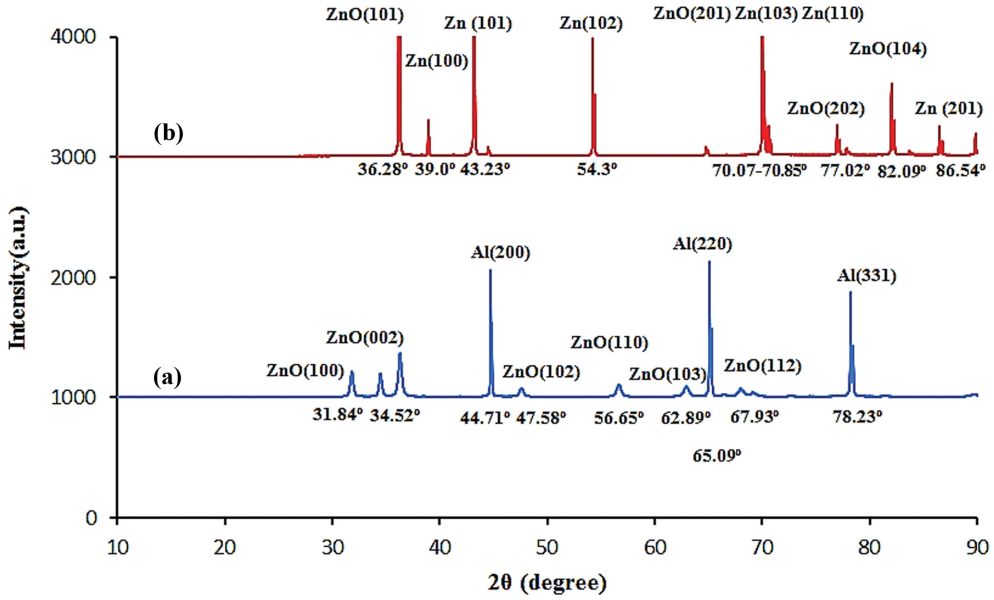


Fig. 7. XRD spectra of Zn coatings formed by spray pyrolysis at (a) 0.25 M, (b) 0.4 M concentration.

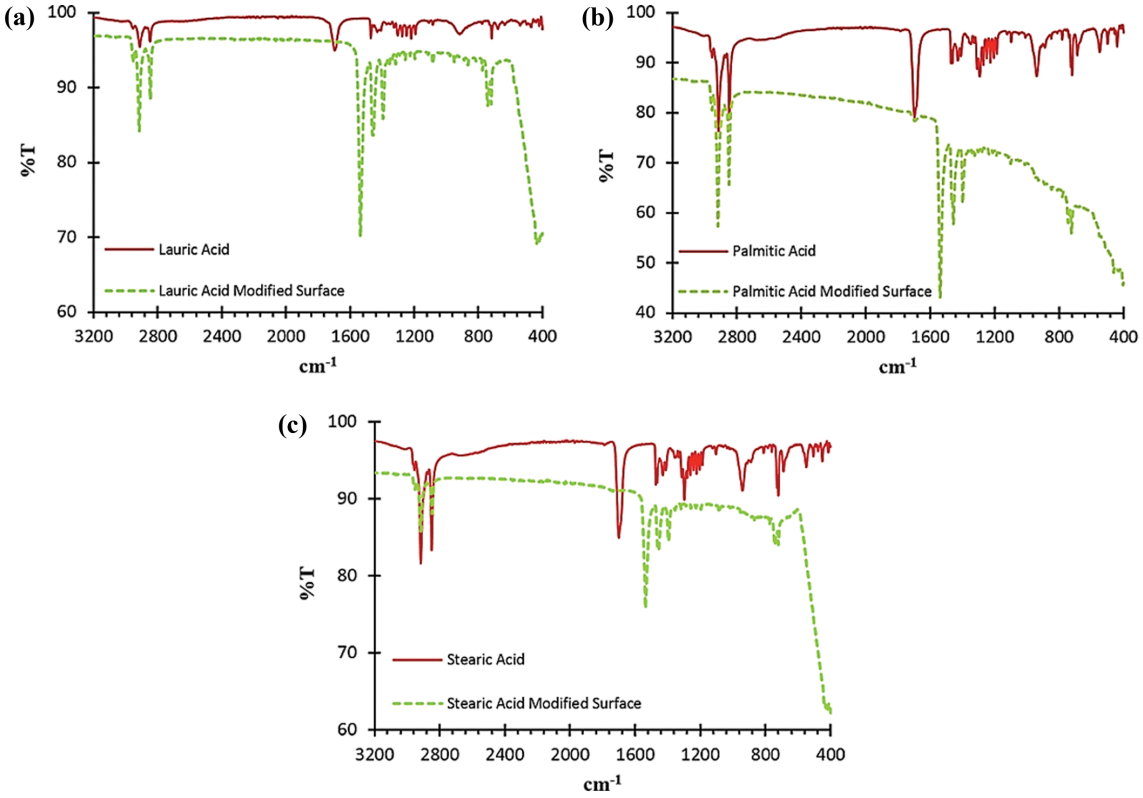


Fig. 8. FT-IR spectrum of the (a) lauric acid, (b) palmitic acid, (c) stearic acid modified samples.

predicted that the actual micro and nano-roughness is provided after spray coating. We can say that anodizing has prepared the ground for this coating and has created patterned roughness for the coating to be more durable depending on time.

XRD analysis was used to obtain information about the crystal structure of particles on the surface after coating. The XRD spectra of the coatings obtained by using 15 ml, 0.25 M and 15 ml, 0.4 M $ZnNO_3$ solutions are presented in Fig. 7.

The structure of the surface coated with 0.4 M and 15 ml solution is indexed as follows: ZnO (101), ZnO (202), ZnO (104) at the peaks at 2θ=36.3°, 77.02° and 82.1°, respectively. Similarly, metallic Zn in the structure is indexed as Zn (100), Zn (101), Zn (102), Zn (201) at the peaks of 2θ=39.0°, 43.2°, 54.3° and 86.54°, respectively. ZnO (201), Zn (103), Zn (110) peaks are located at 2θ=70°, where Zn and ZnO structures are indexed at almost the same place [50-59]. Similarly, the structure of the surface coated with 0.25 M and 15 ml solution is indexed as follows: ZnO (100), ZnO (002), ZnO (101), ZnO (102), ZnO (110), ZnO (103), ZnO (200), ZnO (112), ZnO (201), ZnO (202) at the peaks at 2θ=31.84°, 34.52°, 36.29°, 47.58°, 56.65°, 62.89°, 66.41°, 67.93°, 69.18° and 77.01°, respectively [60-63]. All characteristic peaks of ZnO in the structure agree well with the data of the Joint Committee on Powder Diffraction Standards (JCPDS). In addition, the diffraction peaks associated with the impurity are not observed, confirming the high purity of the coating obtained. As can be seen from the spectrum in Fig. 7(a), both Zn and ZnO structures are formed on the aluminum substrate. In some points Zn and ZnO structures are attributed together. When dilute solution was used, structures such as ZnO (100), ZnO (002), ZnO (102), ZnO (110) were observed. The coating obtained with this solution formed a very thin film; the presence of an aluminum structure was also observed. As the concentration of the solution was increased, the aluminum structure was minimized. At the same time, Zn and ZnO structures were increased.

FT-IR is a characterization technique used for the detection of functional groups. The FTIR spectrophotometer was used to analyze the functional group of samples coated with spray pyrolysis and then modified with solutions of lauric acid, palmitic acid and stearic acid. The analysis of the functional groups of the prepared coatings was carried out using the ATR technique in the frequency range 4,000-400 cm^{-1} and shown in Fig. 8. The FTIR spectra of the fatty acids and post-modification surfaces are given separately in each graph for comparison. Dense peaks at 2,914 cm^{-1} and 2,846 cm^{-1} are associated with -CH_n groups. These peaks refer to the symmetric and asymmetric stress vibration of the long alkyl groups. The characteristic peak COO of acids around 1,700 cm^{-1} shows a shift on modified surfaces and appears as two peaks around 1,450 and 1,530 cm^{-1}. This proves that metallic soap structures were formed on the surface of the coating after the modification. The maximum trend at 400 cm^{-1} indicates the presence of Zn oxide in the structure.

After this stage, SEM images of the modified samples are exhibited in Fig. 9. It is observed that micro/nano modified zinc structures are formed from the morphological properties of the prepared coatings. The surface structure depends on the solution concentration and fatty acid chain length. While high roughness is seen in

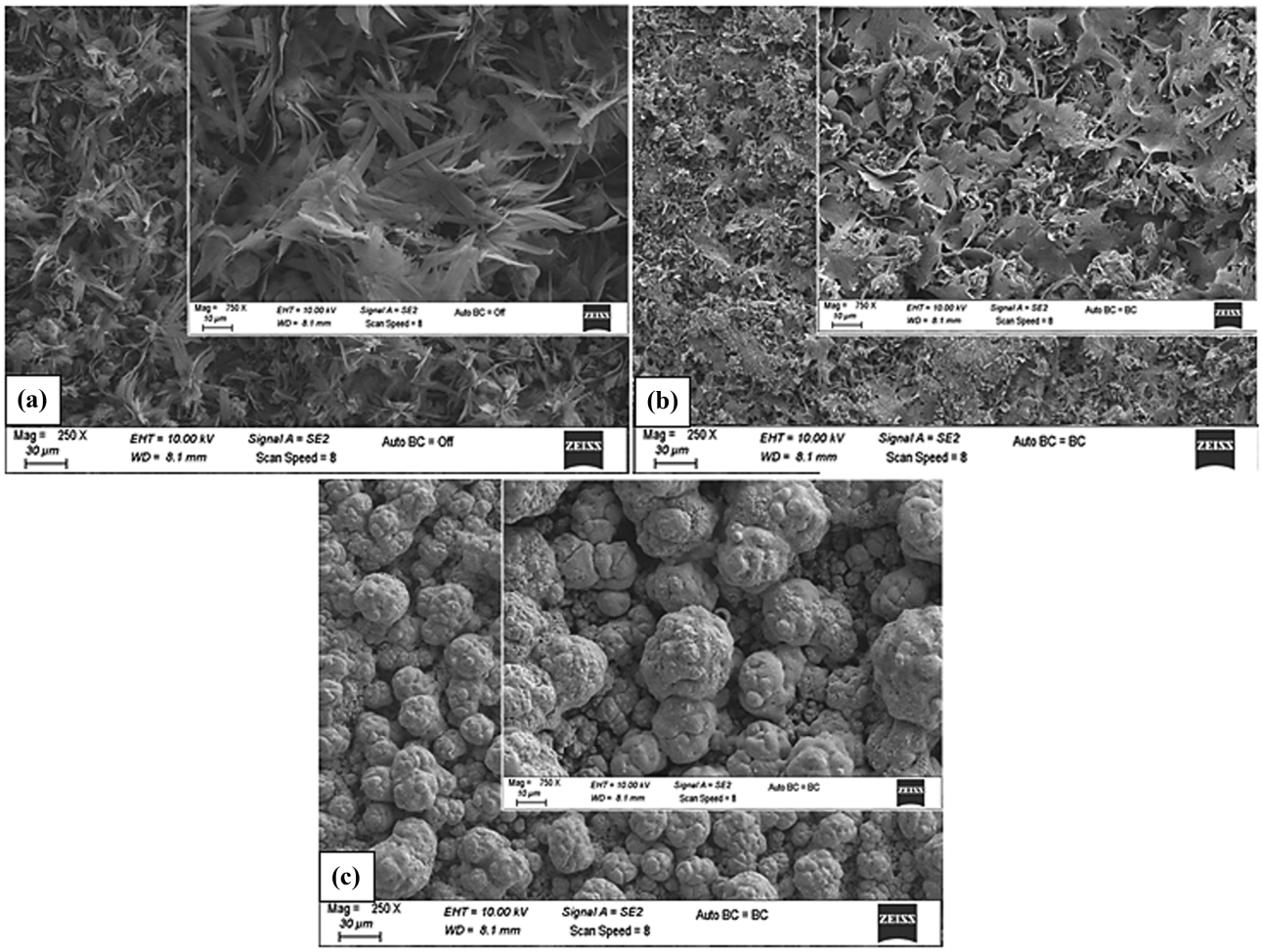


Fig. 9. SEM images of the modified ZnO coatings (a) lauric acid (b) palmitic acid (c) stearic acid.

Fig. 9(a), it is seen in Fig. 9(b) that the roughness decreases and the particle dimensions increase. Spraying at a low concentration made the rod-like structures narrow and homogeneous, but on the other hand, leafier structures emerged in Fig. 9(b). When Fig. 9(b) and (c) were compared, although they were exposed to the same coating conditions, since they were modified with different acids, the surface morphologies were completely different. The leafy structure on the palmitic modified surface appeared while spherical shapes on the stearic acid modified surface. Stearic acid forms spherical structures on the surface, which permits a perfect place for air gaps.

4. Durability

The chemical and mechanical durability of the surface has critical importance for real-world applications. For this reason, samples were subjected to extreme test conditions. The coatings were exposed to UV, temperature, pH medium, and abrasion tests. UV radiation tests were conducted at a wavelength of 368 nm. 5 cm distance was set between the plates and the lamp. The chemical durability of the samples was investigated and compared by immersing the samples in a buffer solution prepared at various pH levels. Temperature experiments were carried out at 100 °C to investigate sample durability as a function of time. Fig. 10(a) shows how the contact angles change by UV exposure with time. The stearic modified coating shows the best performance. Fig. 10(b) shows that samples exposed to high temperatures have a similar tendency.

The surfaces were subjected to a sandpaper abrasion test. Results are demonstrated in Fig. 10(c). The abrasion process mechanically removed the coating on the plate's surface. The modified lauric plates lost their superhydrophobic properties after about 30 cycles. The stearic acid modified plate was more resistant to sanding than the other fatty acids, but it also lost its properties after 80 cycles.

The chemical resistance of samples immersed in the buffer solutions prepared at various pHs was the final test in this section. Surfaces modified with lauric and palmitic acid rapidly lost their properties at high pH (>11), as shown in the Fig. 11. However, stearic acid modified surfaces showed durability for a long time. Samples modified with lauric acid and palmitic acid responded similarly in experiments at pH 1-9 and lost their properties between 40 and 60 minutes. Stearic acid also lasted about 100 minutes in this range.

CONCLUSIONS

Synthesis of superhydrophobic surfaces that is durable for envi-

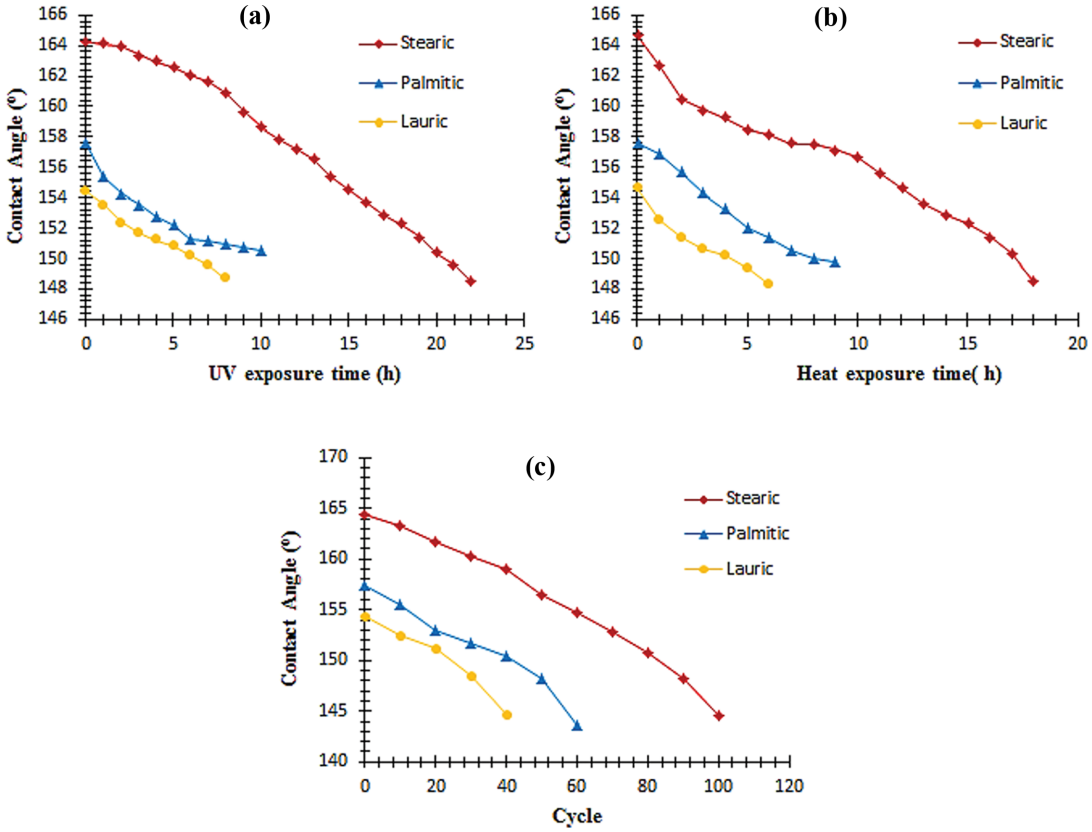


Fig. 10. Contact angle values after (a) UV exposure (b) heat exposure (c) sandpaper abrasion test.

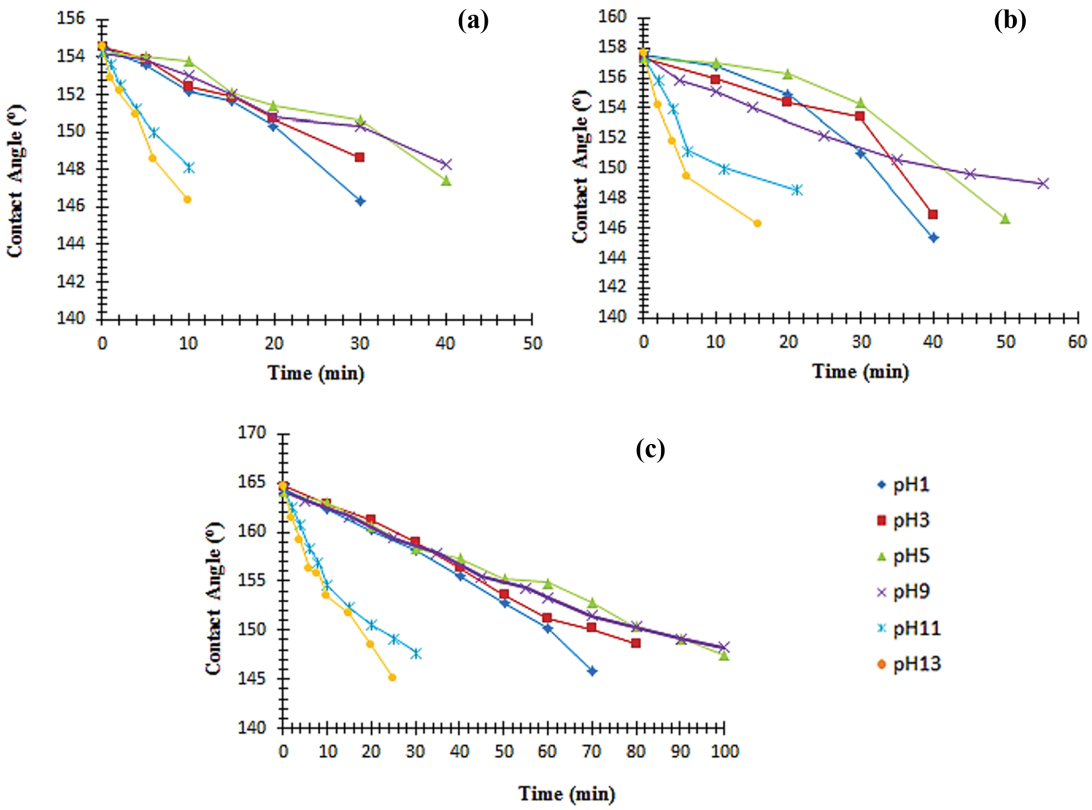


Fig. 11. pH test results for (a) lauric (b) palmitic (c) stearic acid modified samples.

ronmental and operating conditions, aluminum plates are anodized before the ZnO coating. Anodizing time was found to be 10 minutes as optimum for each fatty acid. The samples coated with ZnO by spray pyrolysis method were then modified with fatty acids with different chain lengths. Process parameters were optimized for each fatty acid. The surfaces with the highest contact angle were characterized by various analysis techniques. Chemical and mechanical tests were applied to surfaces modified with different fatty acids under extreme conditions. The best values were found as 154.5°±0.2, 157.5°±0.2, 164.5°±0.2 for lauric, palmitic and stearic acid modified surfaces, respectively. Stearic acid modified surface preserved its super hydrophobicity up to 20 hours under UV light, while lauric lasted 6 hours and palmitic 10 hours. Likewise, the stearic acid modified surface exhibited superhydrophobic property at 100 °C for 17 hours. This time was measured as 4 and 7 hours for lauric and palmitic acid modified surfaces. Modified surfaces could withstand the abrasion test 20, 40 and 80 cycles, respectively. This is a very challenging test and stearic acid demonstrated superior performance here again. In general, it was observed that the superhydrophobic properties decreased rapidly in tests conducted at high pH. For the tests applied at other pH's, lauric, palmitic and stearic were able to stand 20, 30 and 60 minutes resistance.

DECLARATION OF COMPETING INTEREST

The authors declare that they have no known competing financial interests or personal relationships that could have appeared to influence the work reported in this paper.

SUPPORTING INFORMATION

Additional information as noted in the text. This information is available via the Internet at http://www.springer.com/chemistry/journal/11814.

REFERENCES

1. J.-M. Lim, G.-R. Yi, J. H. Moon, C.-J. Heo and S.-M. Yang, *Langmuir*, **23**, 7981 (2007).
2. D.-E. Lee, E.-Y. Choi, H.-J. Yang, A. S. N. Murthy, T. Singh, J.-M. Lim and J. Im, *J. Colloid Interface Sci.*, **555**, 532 (2019).
3. A. Lafuma and D. Quéré, *Nat. Mater.*, **2**, 457 (2003).
4. X. Tan, Z. Huang, L. Jiang, T. Xiao, Y. Wang, X. Yang, H. Zhu, S. Li and X. Chen, *J. Mater. Res.*, **36**, 637 (2021).
5. D. Wang, Q. Sun, M. J. Hokkanen, C. Zhang, F. Y. Lin, Q. Liu, S. P. Zhu, T. Zhou, Q. Chang, B. He, Q. Zhou, L. Chen, Z. Wang, R. H. A. Ras and X. Deng, *Nature*, **582**, 55 (2020).
6. M. O. Penna, A. A. Silva, F. F. do Rosário, S. De Souza Camargo and B. G. Soares, *Mater. Chem. Phys.*, **255**, 123543 (2020).
7. R. Jain and R. Pitchumani, *Langmuir*, **34**(10), 3159 (2018).
8. K. Y. Eum, I. Phiri, J. W. Kim, W. S. Choi, J. M. Ko and H. Jung, *Korean J. Chem. Eng.*, **36**, 1313 (2019).
9. B. Bhushan, in Springer Ser. Mater. Sci., 259 (2018).
10. S.-Y. Li, X.-G. Xiang, B.-H. Ma and X.-D. Meng, *J. Alloys Compd.*, **779**, 219 (2019).
11. J. Li, Z. Jing, F. Zha, Y. Yang, Q. Wang and Z. Lei, *ACS Appl. Mater. Interfaces*, **6**, 8868 (2014).
12. J. Wu, J. Chen, J. Xia, W. Lei and B. Wang, *Adv. Mater. Sci. Eng.*, **2013**, 232681 (2013).
13. N. Agrawal, S. Munjal, M. Z. Ansari and N. Khare, *Ceram. Int.*, **43**, 14271 (2017).
14. P. Nguyen-Tri, H. N. Tran, C. O. Plamondon, L. Tuduri, D. V. N. Vo, S. Nanda, A. Mishra, H. P. Chao and A. K. Bajpai, *Prog. Org. Coatings*, **132**, 235 (2019).
15. X. Li, S. Yin and H. Luo, *Vacuum*, **181**(June), 109674 (2020).
16. W. Liang, X. Sui, X. Zhang, L. He, andY. Sun, *Surf. Innov.*, **8**, 28 (2020).
17. P. Nguyen-Tri, F. Altiparmak, N. Nguyen, L. Tuduri, C. M. Ouellet-Plamondon and R. E. Prud'Homme, *ACS Omega*, **4**, 7829 (2019).
18. X. J. Guo, C. H. Xue, S. Sathasivam, K. Page, G. He, J. Guo, P. Promdet, F. L. Heale, C. J. Carmalt and I. P. Parkin, *J. Mater. Chem. A*, **7**, 17604 (2019).
19. D. G. Kim, T. H. Kim and K. C. Song, *Korean J. Chem. Eng.*, **38**, 635 (2021).
20. X. Li, S. Yin, S. Huang, H. Luo, and Q. Tang, *Vacuum*, **173**, 109172 (2020).
21. C. Chen, Y. He, Y. Fan, X. Chen and Q. Yang, *Surf. Innov.*, **6**, 106 (2017).
22. M. Zhong, Y. Zhang, X. Li and X. Wu, *Surf. Coatings Technol.*, **347**, 191 (2018).
23. M. E. Mohamed and B. A. Abd-El-Nabey, *ECS J. Solid State Sci. Technol.*, **9**, 061006 (2020).
24. J. Zhu, *Appl. Surf. Sci.*, **447**, 363 (2018).
25. F. Huang, Q. Li, G. Ji, J. Tu, N. Ding, Q. Qu and G. Liu, *Mater. Chem. Phys.*, **266**, 124493 (2021).
26. T. A. Khattab, A. L. Mohamed and A. G. Hassabo, *Mater. Chem. Phys.*, **249**, 122981 (2020).
27. J. Zhang, Z. Liu, J. Liu, L. E and Z. Liu, *Mater. Chem. Phys.*, **183**, 306 (2016).
28. M. Liravi, H. Pakzad, A. Moosavi and A. Nouri-Borujerdi, *Prog. Org. Coatings*, **140**, 105537 (2020).
29. Y. Fan, Y. He, P. Luo, X. Chen, Z. Yu and M. Li, *Mater. Lett.*, **188**, 115 (2017).
30. J. Zhu and X. Hu, *J. Coatings Technol. Res.*, **16**, 249 (2019).
31. J. Lomga, P. Varshney, D. Nanda, M. Satapathy, S. S. Mohapatra and A. Kumar, *J. Alloys Compd.*, **702**, 161 (2017).
32. N. Celik, I. Torun, M. Ruzi, A. Esidir and M. S. Onses, *Chem. Eng. J.*, **396**, 125230 (2020).
33. S. Wang, J. Sha, W. Wang, C. Qin, W. Li and C. Qin, *Carbohydr. Polym.*, **195**, 39 (2018).
34. K. Golovin, M. Boban, J. M. Mabry and A. Tuteja, *ACS Appl. Mater. Interfaces*, **9**, 11212 (2017).
35. I. Torun, N. Celik, M. Ruzi and M. S. Onses, *Surf. Coatings Technol.*, **405**, 126543 (2021).
36. C. Wang, F. Tang, Q. Li, Y. Zhang and X. Wang, *Colloids Surfaces A Physicochem. Eng. Asp.*, **514**, 236 (2017).
37. S. Zhang, W. Li, W. Wang, S. Wang and C. Qin, *Appl. Surf. Sci.*, **497**, 143816 (2019).
38. A. Bake, N. Merah, A. Matin, M. Gondal, T. Qahtan and N. Abu-Dheir, *Prog. Org. Coatings*, **122**, 170 (2018).
39. E. Taghvaei, A. Moosavi, A. Nouri-Borujerdi, M. A. Daeian and S.

Vafaeinejad, *Energy*, **125**, 1 (2017).
40. Z. Huang, R. S. Gurney, T. Wang and D. Liu, *J. Colloid Interface Sci.*, **527**, 107 (2018).
41. X. Li, S. Zhao, W. Hu, X. Zhang, L. Pei and Z. Wang, *Appl. Surf. Sci.*, **481**, 374 (2019).
42. M. Cui, Y. Shen, H. Tian, Y. Yang, H. Feng and J. Li, *Surf. Coatings Technol.*, **347**, 38 (2018).
43. R. Zhang, P. Hao, X. Zhang and F. He, *Int. J. Heat Mass Transf.*, **122**, 395 (2018).
44. J. Sun, H. Li, Y. Huang, X. Zheng, Y. Liu, J. Zhuang and D. Wu, *ACS Omega*, **4**, 2750 (2019).
45. R. Zhang, P. Hao and F. He, *Langmuir*, **33**, 3556 (2017).
46. M. T. Li, M. Liu, Y. H. Yu, A. W. Li and H. B. Sun, *Bull. Chem. Soc. Jpn.*, **92**, 283 (2019).
47. N. Ma, Y. Chen, S. Zhao, J. Li, B. Shan and J. Sun, *Surf. Eng.*, **35**, 394 (2019).
48. J. Ma, X. Zhang, Y. Bao and J. Liu, *Colloids Surfaces A Physicochem. Eng. Asp.*, **472**, 21 (2015).
49. D. Ebert and B. Bhushan, *J. Colloid Interface Sci.*, **384**, 182 (2012).
50. A. Goux, T. Pauporté, J. Chivot and D. Lincot, *Electrochim. Acta*, **50**, 2239 (2005).
51. N. Ahmed, A. Majid, M. A. Khan, M. Rashid, Z. A. Umar and M. A. Baig, *Mater. Sci.*, **36**, 501 (2018).
52. K. Zarşbska, M. Kwiatkowski, M. Gniadek and M. Skompska, *Electrochim. Acta*, **98**, 255 (2013).
53. Z. Liu, L E, J. Ya and Y. Xin, *Appl. Surf. Sci.*, **255**, 6415 (2009).
54. A. Bragaru, M. Kusko, E. Vasile, M. Simion, M. Danila, T. Ignat, I. Mihalache, R. Pascu and F. Craciunoiu, *J. Nanoparticle Res.*, **15**, 1352 (2013).
55. L. Hao, Y. Sirong and H. Xiangxiang, *New J. Chem.*, **39**, 4860 (2015).
56. S. Jiao, L. Xu, K. Hu, J. Li, S. Gao and D. Xu, *J. Phys. Chem. C*, **114**, 269 (2010).
57. N. Ait Ahmed, H. Hammache, M. Eyraud, C. Chassigneux, P. Knauth, A. lahreche, L. Makhloufi and N. Gabouze, *Ionics (Kiel)*, **24**, 277 (2018).
58. O. Lupan, L. Chow, G. Chai and H. Heinrich, *Chem. Phys. Lett.*, **465**, 249 (2008).
59. X. F. Lei and J. X. Ma, *J. Braz. Chem. Soc.*, **21**, 209 (2010).
60. W. Muhammad, N. Ullah, M. Haroon and B. H. Abbasi, *RSC Adv.*, **9**, 29541 (2019).
61. M. R. Arefi and S. Rezaei-Zarchi, *Int. J. Mol. Sci.*, **13**, 4340 (2012).
62. S. D. Lee, S. H. Nam, M. H. Kim and J. H. Boo, *Phys. Procedia*, **32**, 320 (2012).
63. A. Khorsand Zak, R. Razali, W. H. Abd Majid and M. Darroudi, *Int. J. Nanomedicine*, **6**, 1399 (2011).

Supporting Information

Highly durable spray-coated superhydrophobic surface: Pre-anodizing and fatty acid chain length effect

Omur Aras, Enver Baydir†, and Bugra Akman

Bursa Technical University, Faculty of Engineering and Natural Sciences, Department of Chemical Engineering, Turkey
(*Received 4 July 2021 • Revised 19 August 2021 • Accepted 5 September 2021*)

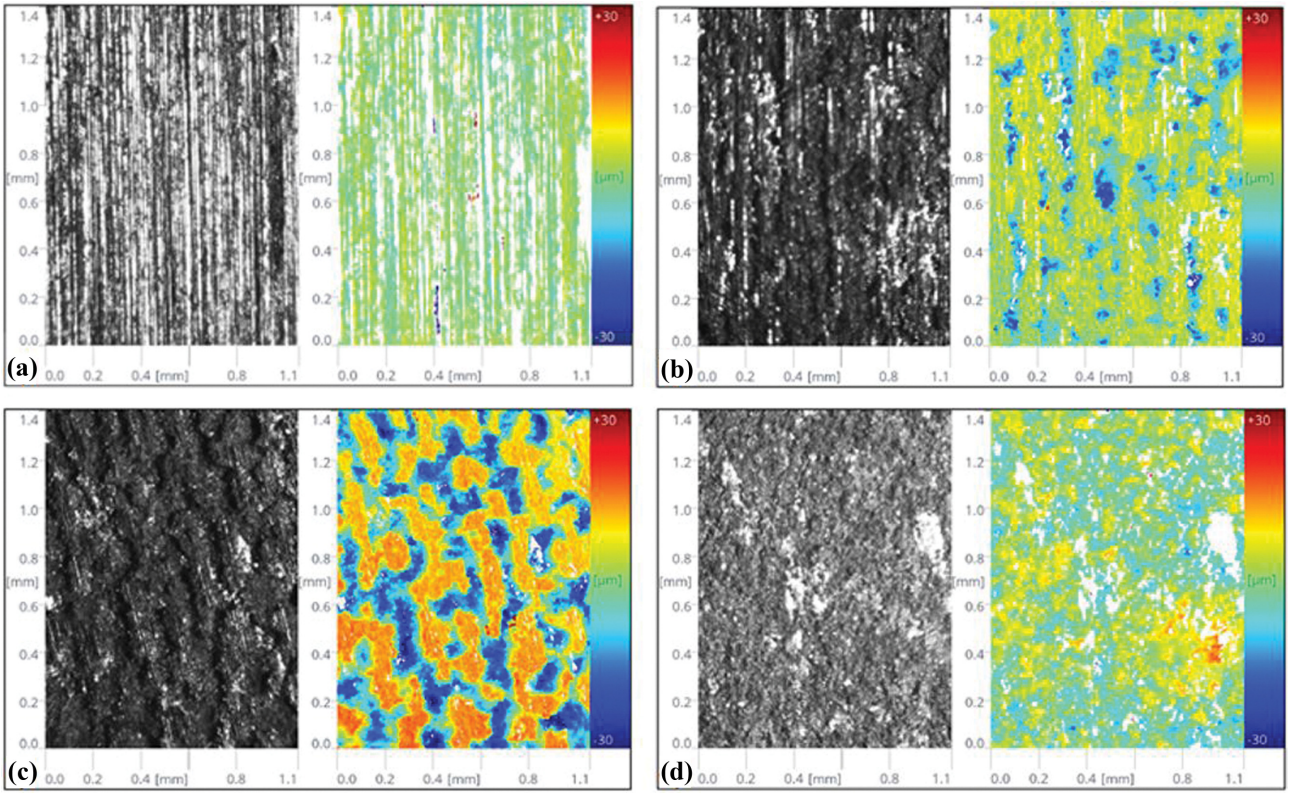


Fig. S1. Surface topography of the samples after the anodizing (a) 1 minute, (b) 5 minutes, (c) 10 minutes, (d) 25 minutes.

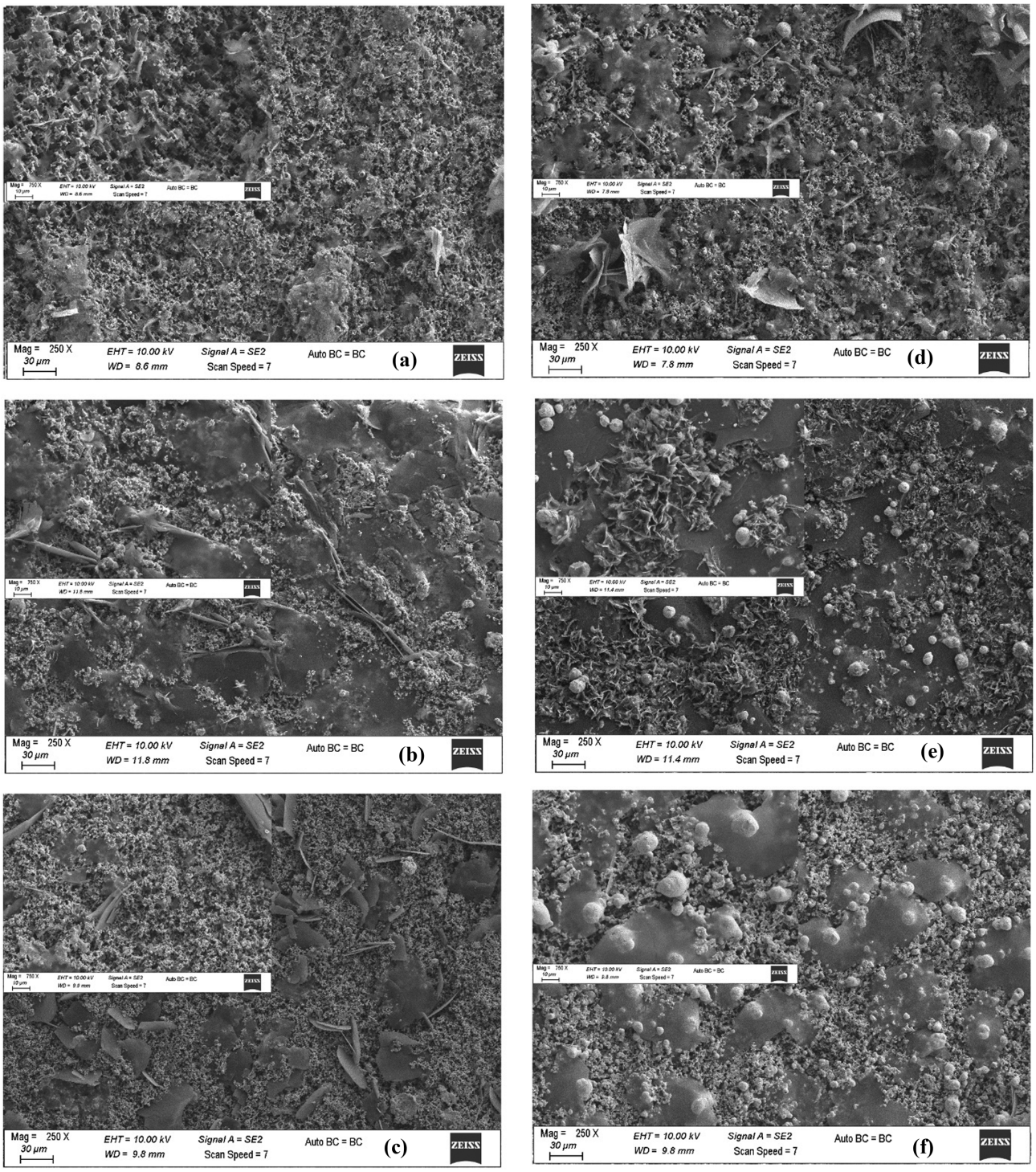


Fig. S2. Solution concentration and fatty acid chain length effect on surface structure.

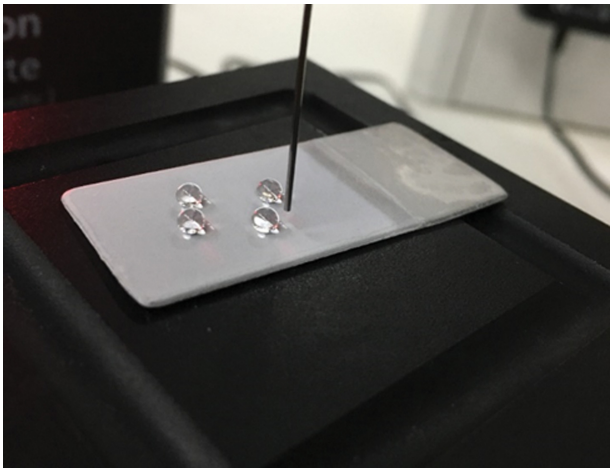


Fig. S3. Superhydrophobic surface obtained by stearic modification.

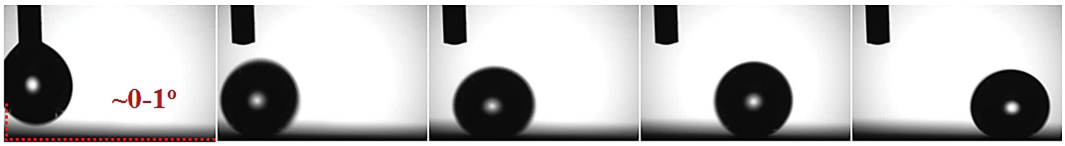


Fig. S4. Sliding angle of the stearic acid modified surface.

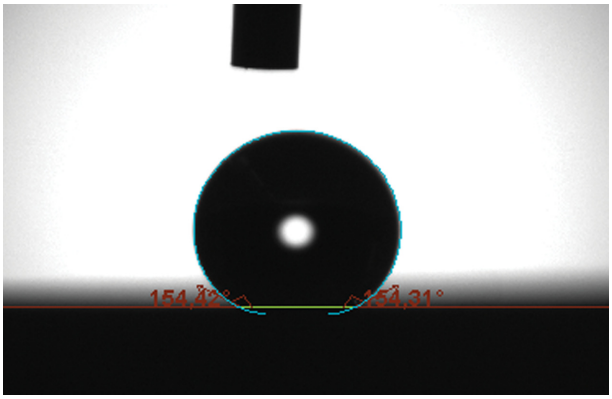


Fig. S5. Lauric's-best-result.

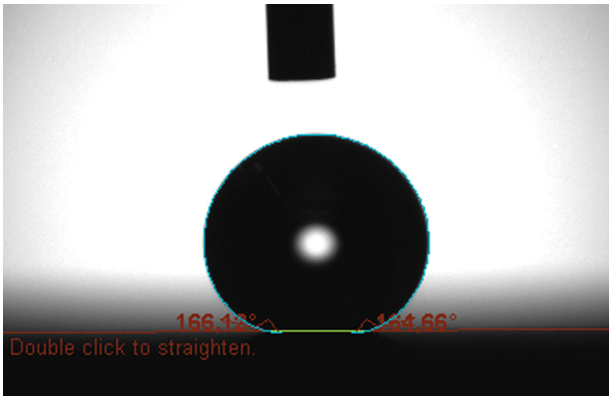


Fig. S7. Stearic's-best-result.

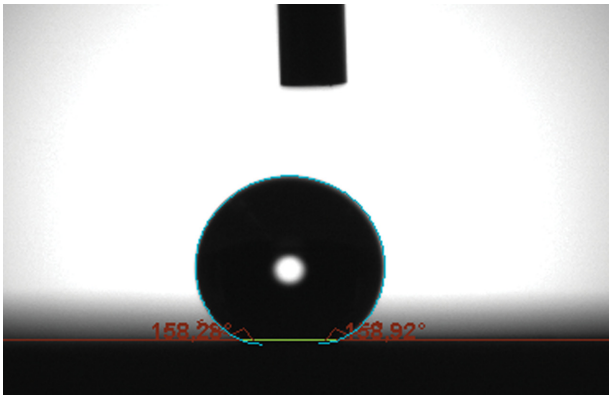


Fig. S6. Palmitic's best result.